PHYSICAL REVIEW A **79**, 041201(R) (2009)

Ionization and charge migration through strong internal fields in clusters exposed to intense x-ray pulses

Christian Gnodtke, Ulf Saalmann, and Jan M. Rost
Max Planck Institute for the Physics of Complex Systems, Nöthnitzer Straße 38, 01187 Dresden, Germany and Max Planck Advanced Study Group at the Center for Free-Electron Laser Science, Luruper Chaussee 149, 22761 Hamburg, Germany

(Received 11 December 2008; published 27 April 2009)

A general scenario for electronic charge migration in finite samples illuminated by an intense laser pulse is given. Microscopic calculations for neon clusters under strong short pulses as produced by x-ray free-electron laser sources confirm this scenario and point to the prominent role of field ionization by strong internal fields. The latter leads to the fast formation of a core-shell system with an almost static core of screened ions while the outer shell explodes. Substituting the shell ions with a different material such as helium as a sacrificial layer leads to a substantial improvement of the diffraction image for the embedded cluster thus reducing the consequences of radiation damage for coherent diffractive imaging.

DOI: 10.1103/PhysRevA.79.041201 PACS number(s): 36.40.Wa, 87.59.−e, 87.15.ht, 41.60.Cr

The advent of sources producing short and intense pulses of light with frequencies ranging from soft to hard x rays [1] opens a new parameter regime for light-matter interaction. Dynamics with a quick removal of many electrons from their bound states in the atoms of the sample irradiated has scarcely been explored before. It is important to have a good insight into this dynamics in order to realize one of the goals of x-ray free-electron lasers (XFELs) which deliver such light pulses: the single-shot coherent diffractive imaging of finite samples with atomic resolution [2]. X-ray photons scatter elastically from a single nonperiodic molecule, such as a protein, and are subsequently recorded on a charge-coupled device (CCD) as a continuous diffraction pattern [3]. The estimated total photon flux required for single-shot diffraction imaging exceeds 10^{12} photons per $(100\ \mathrm{nm})^2$ [3–5] and is at the limit of what XFELs can deliver. Above all, such high photon fluxes lead to radiation damage by multiple ionization and subsequent Coulomb explosion of the sample which degrades the diffraction image if not destroys it.

For possible means to overcome this handicap a detailed understanding of the time-dependent multiparticle dynamics is required which is very interesting in its own right. Apart from simulations in the x-ray regime [3,6–11], this problem has been approached from the perspective of intense long-wavelength laser pulses. There, it was found that finite systems, such as atomic clusters or nanodroplets, display behavior fundamentally different from single atoms or bulk systems [12,13]. The large space charge of ions in a finite volume creates strong electric fields easily exceeding the strong external field of the laser. Similarly, very strong internal fields are generated by single-photon ionization in x-ray pulses since many photoelectrons can leave the sample due to the high photon energy. In both cases the strong internal field leads to the release of additional electrons, mainly from the surface. In the x-ray regime this effect has profound consequences for diffractive imaging, as we will show.

As long as the laser frequency is sufficiently high to trigger initial ionization, a unified scenario with four phases emerges for a sample illuminated by an intense light pulse. (i) Electrons are photodetached from the atoms by the laser and leave the cluster. (ii) The substantial ionic charge developed during the first phase generates a large electric field particularly at the cluster surface, leading to almost instantaneous field ionization of surface atoms. These electrons migrate toward the cluster center. (iii) An electron plasma is established, initially formed by field-ionized electrons. For sufficiently large samples secondary electrons (from Auger decay or electron-impact ionization) and even photodetached electrons are trapped by the cluster potential, "feeding" the plasma. (iv) The electron plasma shields the core of the cluster so that only the (highly charged) outer shell explodes.

This scenario occurs for many combinations of parameters (sample size and density, pulse length, frequency, and intensity) provided that the quiver amplitude $x=F/\omega^2$, i.e., the excursion of electrons induced by the oscillating laser field with amplitude F and frequency ω, is much smaller than the characteristic size (linear extension X) of the sample, $x \ll X$. In the x-ray regime [7,9] this is fulfilled even for high-field strengths, but it has been shown to occur also for much smaller frequencies in the vuv [14]. Recently, this electron migration has been elegantly verified experimentally with an *ad hoc* designed core-shell system of a xenon-argon composite cluster [15].

Figure 1 shows at which combination of cluster radius and average charge per ion trapping of photoelectrons and Auger electrons is expected for neon clusters exposed to a 12 keV photon pulse, relevant for atomic-resolution imaging. One sees immediately that large clusters trap even x-ray photoelectrons while samples of moderate size trap only the much slower Auger electrons. Field ionization, in contrast, occurs from the smallest sample sizes on. What contributes even more to their prominent role for the dynamical screening of ions is the fact that the field ionized electrons are not only available in a sample of arbitrary size but they are also the first electrons available for screening once the ionizing laser pulse sets in. Auger electrons, on the other hand, appear only about 2.5 fs after a K-shell photoionization event in neon when the core hole undergoes an Auger decay.

The critical field $\mathcal{E}_c$ for ionization of an atom can be estimated by the Bethe rule [16] $\mathcal{E}_c=E_{ip}^2/(4Z)$, where E_{ip} is the

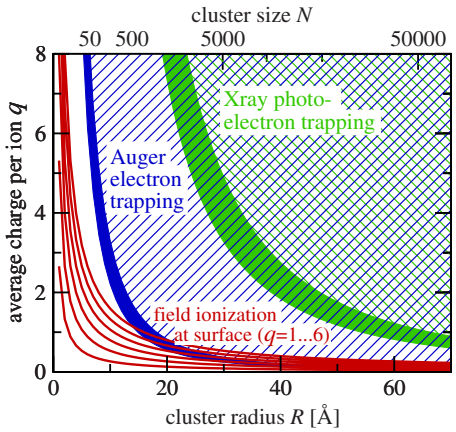

FIG. 1. (Color online) Electron trapping and strong-field effects of homogeneously charged neon clusters with an average charge q per ion and a cluster radius R. Trapping of electrons detached by 12 keV photons (region above and including green/light-gray shaded band) and the Auger decays (region above and including blue/dark-gray shaded band). The thick lower borders take into account that electrons are released from any position in the cluster. Red/solid lines: ionization of surface ions at various charge states ($q=1,\ldots,6$) due to the internal radial field of the charged cluster estimated by the Bethe rule, see text.

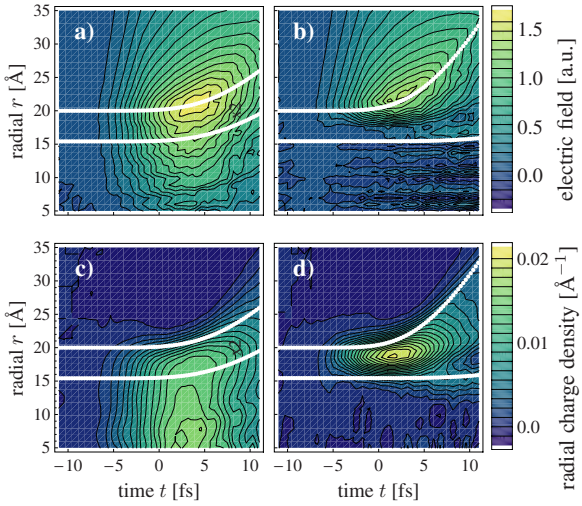

FIG. 2. (Color online) Radial electric field (upper panels) and radial charge density (lower panels) for a Ne_{1500} cluster and $T=10$ fs pulse without the effect of field ionization (left) and with field ionization (right). White lines show the average radial coordinate of cluster surface shell (the 5% outermost ions) and of cluster-core surface shell (the 5% outermost ions of the inner half of the cluster).

ionization potential and Z is the charge of the binding core. Hence, fields produced in neon clusters as small as $R\approx 10$ Å are sufficient for multiple ionization of the surface atoms (red solid lines in Fig. 1), while larger clusters with radii $R\gtrsim 50$ Å reach the critical field strength at the surface with only a small fraction of photoionized atoms. This suggests field ionization as an extremely efficient and fast mechanism for an electron migration that leads to screening of the core of the sample.

To assess the effect of field ionization quantitatively we have calculated the dynamics of neon clusters of $N=50$ ($R\approx 6$ Å) up to $N=15000$ ($R\approx 42$ Å) atoms under intense, short ($T=1,\ldots,20$ fs) pulses with a photon energy of $E_{\mathrm{ph}}=12$ keV focused to an area of $A=(100\ \mathrm{nm})^2$. The pulse amplitude in time is given by

$$F(t)=\sqrt{I_{\mathrm{peak}}}\cos^2\left(c\frac{t}{T}\right)\quad\text{for}\quad |t|\le(\pi T)/(2c),\qquad(1)$$

with $c=2\arccos(2^{-1/4})\approx 1.144$ so that T has the meaning of the full width at half maximum pulse length of the intensity $I(t)=F^2(t)$. For a fixed number of $n=10^{12}$ photons in the pulse, the peak intensity follows as

$$I_{\mathrm{peak}}=\frac{nE_{\mathrm{ph}}}{TA}=\frac{1.92}{T/\mathrm{fs}}10^{22}\ \mathrm{W/cm^2}.\qquad(2)$$

Note that for different pulse lengths T, as discussed below, the peak intensity I_{peak} changes. Our approach is based on a classical molecular-dynamics simulation similar to the one described in [6,17], with photoionization and Auger decay treated by quantum-mechanical rates. The important effect of field ionization is included by always propagating the least bound electron of each atom or ion as a classical particle in the field of all other ions and electrons. An ionization event is taken to have occurred when this electron leaves its mother ion beyond a threshold radius. We have found the system dynamics to be insensitive to the particular choice of threshold radius, so long as we stay within the natural limits of half the nearest-neighbor distance from above and a minimum radius which avoids counting bound electrons with large excursion radius as ionized despite their immediate return to the allowed region. Within this range we have settled on the threshold radius value of 2.2 a.u.. Our approach has the advantage of incorporating the total field of all charged particles, therefore including both electron-impact ionization and ionization due to static fields [18]. We made use of an implementation [19] of the fast-multipole method [20] to calculate the Coulomb interaction of electrons and ions in order to bring calculation times for the larger systems to a manageable level.

Paradigmatically, we first consider a Ne_{1500} cluster under a 10 fs pulse. To clearly identify the effect of field ionization, we have performed two calculations for each parameter set. A full calculation including ionization from quasistatic internal fields and a reduced calculation without this effect. The latter amounts in our approach to exclude the classical propagation of a bound $2p$ electron with every atom or ion. At peak intensity, halfway through the pulse roughly each atom will have been singly photoionized. However, with a radius of $R\approx 20$ Å this cluster is not yet large enough to capture any of the photoelectrons, cf. Fig. 1. Without field ionization this leads to a homogeneous charging of the cluster, see Fig. 2(c). The resulting electric field [Fig. 2(a)] exhibits a linear increase inside the cluster and a $1/r$ dependence outside the cluster. The maximum field at the surface is about 1.5 a.u. which is sufficiently high for further ionization and should not be neglected.

Field ionization generates many plasma electrons in the cluster. More specifically, at peak intensity there will already

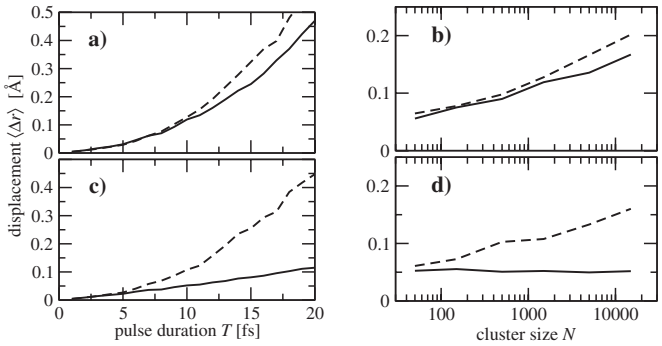

FIG. 3. Mean displacement of ions $\langle \Delta r \rangle$ of neon clusters at peak intensity ($t=0$) for a full calculation (solid lines) and reduced calculations (dashed lines) neglecting field ionization. Dependence on the pulse duration T (left, for Ne_{1500}) and the cluster size N (right, $T=10$ fs), respectively. The average $\langle \Delta r \rangle$ is shown for all cluster ions in the upper panels and for only the inner half of the cluster ions in the lower panels.

be an average of two plasma electrons per cluster ion created in this way. Thereby, the cluster effectively becomes a charged conducting sphere: the electrons neutralize the ionic charges at the center of the cluster and the excess positive charge is localized on the surface as can be seen in Fig. 2(d) in accordance with phase (iii) described before. As anticipated, this highly efficient charge migration begins almost immediately with the photoinduced charging of the cluster and takes place on a subfemtosecond time scale preceding the trapping of Auger electrons as K-shell holes decay much more slowly. The emergence of a neutral core with a positively charged shell leads to a fundamentally different electric field, as is shown in Fig. 2(b): although the field at the surface is of similar strength as in the homogeneously charged cluster, there is now a nearly field-free region in the cluster center. Within this region the ion motion is therefore drastically suppressed at the expense of a violent explosion of the more strongly charged outer shell.

The averaged radial trajectories of the surface ions starting at $r \approx R$ and of the shell enclosing the inner half of the cluster ions starting at $r \approx R/2^{1/3}$ (white lines in Fig. 2) indicate this twofold dynamics of the cluster ions. Clearly and in contrast to the reduced calculation, the cluster core in the full calculation displays almost no expansion throughout the pulse.

The mean displacement,

$$\langle \Delta r \rangle = \frac{1}{N} \sum_{i=1}^{N} |\vec{r}_i(-\infty) - \vec{r}_i(0)|, \tag{3}$$

of the ions from their initial positions ($t \to -\infty$) provides a systematic and more quantitative measure of the effect of charge migration and its dependence on pulse duration T and sample size N. It is shown in Fig. 3(a) for various pulse lengths T (but a fixed photon number per pulse) in the full and reduced calculations at $t=0$, the time of peak intensity from which the largest contribution to the diffraction pattern in an imaging experiment can be expected. We find a strong amplification of ionic motion with increasing pulse length. Two factors contribute to this increase. First, a longer pulse obviously means a longer propagation of an ion with its acquired momentum, and second the charging of the cluster is higher for the longer pulses due to the inherent time scale of about 2.5 fs set by the Auger decay. Although the constant total photon number n means that at peak intensity each atom will have undergone roughly one photoionization event for all pulse lengths, clusters under longer pulses will additionally have seen Auger decays. Many of these Auger electrons will escape the cluster, cf. Fig. 1, leading to a higher charging. The induced ion motion depends also on the sample size and shows a strong increase in the mean displacement with increasing cluster size [Fig. 3(b)]. Due to the additive nature of the Coulomb force a larger cluster has larger electrostatic energy density than a smaller cluster of equal charge density. This leads to stronger ionic motion in larger clusters.

As expected, the displacement is up to 20% lower [Fig. 3(a)] in the full calculation since the electrostatic energy of a charged conductor (with the charge localized on the surface) is smaller than that of a homogeneously charged sphere of equal charge. However, the displacement averaged over all ion positions does not reflect the core-shell nature of the cluster ions with the almost static core and the exploding shell in the case of effective field ionization. Therefore, Figs. 3(c) and 3(d) show the displacement for the ionic core (the inner half of the ions) only, revealing a dramatic effect: the mean displacement of the cluster core atoms is reduced by up to 75% for Ne_{1500} for pulses of 20 fs [Fig. 3(c)] and similarly for the larger cluster Ne_{15000} at 10 fs [Fig. 3(d)] length. Yet, there seems to be a lower limit for $\langle \Delta r \rangle$ as is most obvious in Fig. 3(d) but also appears through the almost linear increase with pulse length T in Fig. 3(c). This lower limit is due to the recoil acquired by the neon ions during absorption of the 12 keV photon, which is about 0.017 Å/fs.

The different ion dynamics, split into an inert core and an exploding shell, naturally lead to the idea of a sacrificial layer for imaging experiments as proposed before [10] and further investigated in [21] for carbon-based samples. Due to the different material used the results are not directly comparable. However, the actual dynamics of an exploding shell may be very different in our case since field-ionized electrons are created much faster than those due to electron-impact ionization from the trapped Auger electrons. We consider here a Ne_{1500} cluster embedded in a helium droplet of 15 000 atoms. During its buildup, the net positive charge is efficiently and quickly transferred from the cluster to the droplet. The entire neon cluster now forms the core of the composite system and remains mostly unscathed, while the helium droplet, taking the role of the ionized shell, explodes as can be seen in Fig. 4(a) where $\langle \Delta r \rangle$ is shown for the case with and without the helium droplet.

In the context of coherent diffractive imaging it is important to ascertain that the strong reduction in $\langle \Delta r \rangle$ translates into an equally improved quality of the obtained diffraction pattern. We used our cluster data to calculate the diffraction pattern corresponding to a spatial resolution of 2 Å, where as in previous investigations [10] we neglected contributions from the tamper and the plasma electrons. This diffraction pattern, characterized by the intensity I_i^{real} registered at pixel i of a detector having k pixels, is then compared to an ideal

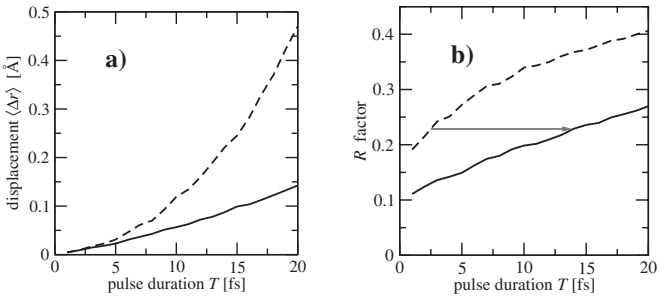

FIG. 4. (a) Mean displacement and (b) R factor of ions of Ne_{1500} cluster embedded in He_{15000} droplet (full line) and without helium droplet (dashed line) for varying pulse lengths. The gray arrow indicates a typical improvement in the damage tolerance, see text.

diffraction pattern I_i^{ideal} without radiation damage. We define

$$R = \sum_{i=1}^{k} |\sqrt{I_i^{\text{real}}} - \sqrt{I_i^{\text{ideal}}}| / \sum_{j=1}^{k} \sqrt{I_j^{\text{ideal}}}, \tag{4}$$

which differs from a previous definition [3] in the normalization of $\sqrt{I_i^{\text{real}}}$. The R factor of Eq. (4) therefore measures discrepancies due to electron loss (either homogeneous or inhomogeneous) and atomic motion. Both influence crucially the image quality which can be obtained with XFEL pulses. In comparison to the pure cluster we find a substantial reduction in the R factor for the helium embedded cluster [Fig. 4(b)]. Much longer pulses are tolerated by the embedded system until a similar level of damage is reached as in the pure cluster. For example, an increase in pulse length by a factor of more than 5 [from $T=2.5$ fs to $T=14$ fs, cf. gray arrow in Fig. 4(b)] becomes possible by embedding the cluster in helium.

We have presented detailed investigations for smaller clusters which have revealed the importance of internal field ionization for subsequent charge migration. For larger clusters ($R \gtrsim 60$ Å) the trapping of photoelectrons becomes possible, and for clusters with radii in the hundreds of Ångström range, most photoelectrons will be trapped. Photoelectron trapping limits the average charge per atom in the cluster and the general rule of the surface field strength linearly increasing with cluster size is no longer valid. A simple estimate using the Bethe rule for this scenario nonetheless still predicts appreciable ionization through quasistatic internal fields. For an $R=250$ Å cluster, for example, in which 50% of the atoms are singly photoionized despite the trapping of most photoelectrons, the surface field will still be sufficient for double ionization of a neutral atom. Hence, the field ionization induced ultrafast charge migration can be expected to play an important role for the success of single-shot coherent diffraction imaging experiments for a wide array of the samples of interest.

[1] J. Feldhaus, J. Arthur, and J. B. Hastings, J. Phys. B **38**, S799 (2005).
[2] K. J. Gaffney and H. N. Chapman, Science **316**, 1444 (2007).
[3] R. Neutze, R. Wouts, D. van der Spoel, E. Weckert, and J. Hajdu, Nature (London) **406**, 752 (2000).
[4] S. P. Hau-Riege, R. A. London, G. Huldt, and H. N. Chapman, Phys. Rev. E **71**, 061919 (2005).
[5] J. Miao, K. O. Hodgson, and D. Sayre, Proc. Natl. Acad. Sci. U.S.A. **98**, 6641 (2001).
[6] U. Saalmann and J. M. Rost, Phys. Rev. Lett. **89**, 143401 (2002).
[7] Z. Jurek, G. Faigel, and M. Tegze, Eur. Phys. J. D **29**, 217 (2004).
[8] Z. Jurek, G. Oszlanyi, and G. Faigel, Europhys. Lett. **65**, 491 (2004).
[9] S. P. Hau-Riege, R. A. London, and A. Szöke, Phys. Rev. E **69**, 051906 (2004).
[10] S. P. Hau-Riege, R. A. London, H. N. Chapman, A. Szoke, and N. Timneanu, Phys. Rev. Lett. **98**, 198302 (2007).
[11] S. P. Hau-Riege and H. N. Chapman, Phys. Rev. E **77**, 041902 (2008).
[12] V. P. Krainov and M. B. Smirnov, Phys. Rep. **370**, 237 (2002).
[13] U. Saalmann, C. Siedschlag, and J. M. Rost, J. Phys. B **39**, R39 (2006).
[14] C. Siedschlag and J. M. Rost, Phys. Rev. Lett. **93**, 043402 (2004).
[15] M. Hoener, C. Bostedt, H. Thomas, L. Landt, E. Eremina, H. Wabnitz, T. Laarmann, R. Treusch, A. R. B. de Castro, and T. Möller, J. Phys. B **41**, 181001 (2008).
[16] H. A. Bethe and E. Salpeter, *Quantum Mechanics of One- and Two-Electron Atoms* (Springer, Berlin, 1957).
[17] A. Mikaberidze, U. Saalmann, and J. M. Rost, Phys. Rev. A **77**, 041201(R) (2008).
[18] C. Gnodtke, U. Saalmann, and J. M. Rost (unpublished).
[19] H. Dachsel and I. Kabadshow, http://www.fz-juelich.de/jsc/fmm.
[20] L. Greengard and V. Rokhlin, J. Comput. Phys. **73**, 325 (1987).
[21] Z. Jurek and G. Faigel, Eur. Phys. J. D **50**, 35 (2008).